Using Two-Dimensional Distributed Feedback for Synchronization of Radiation from Two Parallel-Sheet Electron Beams in a Free-Electron Maser

A. V. Arzhannikov,[1,3] N. S. Ginzburg,[2] P. V. Kalinin,[1,3] S. A. Kuznetsov,[1,3] A. M. Malkin,[2] N. Yu. Peskov,[2] A. S. Sergeev,[2] S. L. Sinitsky,[1,3] V. D. Stepanov,[1] M. Thumm,[3,4] and V. Yu. Zaslavsky[2]

[1]*Budker Institute of Nuclear Physics SB RAS, Novosibirsk 630090, Russia*

[2]*Institute of Applied Physics, Russian Academy of Sciences, Nizhny Novgorod 603950, Russia*

[3]*Novosibirsk State University, Novosibirsk 630090, Russia*

[4]*Karlsruhe Institute of Technology, IHM and IHE, Karlsruhe 76131, Germany*

(Received 7 March 2016; published 6 September 2016)

A spatially extended planar 75 GHz free-electron maser with a hybrid two-mirror resonator consisting of two-dimensional upstream and traditional one-dimensional downstream Bragg reflectors and driven by two parallel-sheet electron beams 0.8 MeV/1 kA has been elaborated. For the highly oversized interaction space (cross section 45×2.5 vacuum wavelengths), the two-dimensional distributed feedback allowed realization of stable narrow-band generation that includes synchronization of emission from both electron beams. As a result, spatially coherent radiation with the output power of 30–50 MW and a pulse duration of ~100 ns was obtained in each channel.

DOI: 10.1103/PhysRevLett.117.114801

Microsecond relativistic electron beams (REBs) of tens of kiloamperes of current and an energy content of hundreds of kilojoules, which are being generated at the Budker Institute of Nuclear Physics (BINP RAS) [1,2], stimulated investigations for generation of ultra-high-power coherent millimeter and submillimeter radiation using such unique beams. An important feature of these beams is the sheet geometry with one of the transverse sizes reaching up to 1.5 m and thus exceeding the wavelength by a few orders of magnitude. The planar geometry of the interaction space is beneficial for a significant increase of the total microwave power while keeping the power density at a moderate level. The key obstacle to realizing generators with a strongly elongated interaction cross section is the provision of coherent emission from various parts of the sheet electron beam.

This problem can be solved based on the concept of two-dimensional distributed feedback (2D DF) [3,4]. This feedback mechanism can be considered as a natural development of a one-dimensional (1D) DF [5–7] widely used currently both in the quantum and classical electronics. In devices of microwave physics, such feedback is realized in metallic waveguides with shallow single-periodic corrugated walls where the Bragg scattering of two partial counterpropagating waves takes place [7]. The new 2D feedback principle implies the use of four partial wave fluxes (Fig. 1)

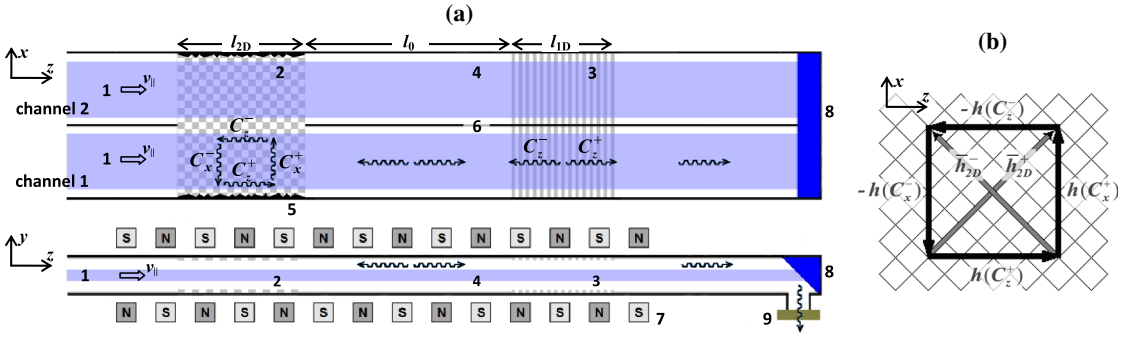

FIG. 1. (a) Schematic of the ELMI experiment to study the synchronization of radiation in a two-beam planar FEM using 2D distributed feedback (top for the x-z plane and bottom for the y-z plane). (1) Parallel-sheet electron beams. (2),(3) 2D upstream and 1D downstream Bragg reflectors. (4) Regular waveguide section. (5) Scatters for transverse wave fluxes. (6) Metal baffle separating different channels. (7) Planar wiggler (shown at the y-z plane). (8) Graphite collector. (9) Output window. (The winding arrows indicate the propagation directions of the partial waves in one of the channels.) (b) Diagram illustrating the scattering of the four partial waves in the 2D Bragg structure ($\vec{\bar{h}}^{\pm}_{2D} = h_{2D}(\vec{x}_0 \pm \vec{z}_0)$ are the gratings vectors).

$$\vec{E} = \vec{E}_0 \mathrm{Re}\{[C_z^+ e^{-ihz} + C_z^- e^{ihz} + C_x^+ e^{-ihx} + C_x^- e^{ihx}] e^{i\omega t}\}, \quad (1)$$

where the two waves with amplitudes $C_z^{\pm}$ propagate in forward and backward $\pm z$ directions (with respect to the electron beam motion) and two other waves with amplitudes $C_x^{\pm}$ propagate in the transverse $\pm x$ directions and act to synchronize radiation from various parts of the sheet electron beam. This feedback mechanism is realized in planar 2D Bragg structures consisting of two metal plates having a gap a_0, width l_x, length l_{2D}, and double-periodical corrugation of the inner surface

$$a = \frac{a_{2D}}{4}[\cos h_{2D}(x - z) + \cos h_{2D}(x + z)], \quad (2)$$

where $a_{2D} \ll (a_0, \lambda)$ is the corrugation depth. Efficient scattering of the partial waves (1) takes place under the Bragg resonance condition

$$h \approx h_{2D}, \quad (3)$$

where $h_{2D} = 2\pi/d_{2D}$ and d_{2D} is the corrugation period over both coordinates [Fig. 1(b)].

Theoretical analysis demonstrates that 2D DF is a rather universal solution that is applicable to different types of active media, including not only large-size electron beams but some laser media as well [8]. The high potential of 2D DF to achieve single-frequency oscillations has been proved experimentally in an oversized coaxial free-electron maser (FEM) operating in the Ka band [9,10] and in a planar FEM operating in the W band [11,12]. Further increase in total FEM radiation power can be achieved by increasing the transverse size of the single-beam generator or by realization of multichannel systems. The second way allows the development of multilayer systems spatially extended over both transverse x and y coordinates or synchronization of a number of independent sources. In particular, the possibility of synchronization of multilayer electron beams moving in parallel over the y coordinate [as it is defined in Fig. 1(a)] in FEMs with 2D DF was simulated in Ref. [13]. In the present work, this possibility of the use of 2D DF in FEMs to provide radiation synchronization has been demonstrated theoretically and experimentally using the simplest two-beam scheme when the channels are arranged in parallel over the x coordinate [Fig. 1(a)].

Experimental studies were performed based on the high-current explosive-emission accelerator ELMI (BINP RAS). In the present experiments [Fig. 1(a)], the oscillator is represented by two parallel FEM sections that are driven by two relativistic sheet electron beams (0.8–1) MeV/(0.5–1) kA/(1–4) μs with the same cross sections of 7 cm $\times$ 0.4 cm. The sheet beams were transported inside two planar vacuum channels with the cross sections of 10 cm $\times$ 0.95 cm by a longitudinal guide magnetic field of up to 1.4 T. The transverse (wiggler) magnetic field component had a spatial period of 4 cm and an amplitude of up to 0.2 T with an adiabatic entrance of 24 cm length.

The microwave system of each FEM section was based on a hybrid two-mirror resonator composed from the upstream 2D and downstream 1D Bragg reflectors separated by a section of regular rectangular waveguide with length $l_0 = 32$ cm. The upstream reflector with length $l_{2D} = 20$ cm consisted of two copper plates with chessboard corrugation with a depth of 0.02 cm and a spatial period $d_{2D} = 0.4$ cm. Theoretical analysis and cold tests showed [11] that the microwave properties of Bragg gratings with such chessboard corrugation are close to those of gratings with ideal 2D sinusoidal corrugation (2). This Bragg structure provided the feedback loop (1) for the four partial waves of TEM type at a frequency close to 75 GHz. The transverse energy fluxes (propagating in $\pm x$ directions) were scattered into high-order waves by metal scatters at the side walls with irregular surface profiles [see Fig. 1(a)]. Since the radiation is amplified by the electron beam mainly after the 2D reflector (see below), the energy losses due to this scattering are relatively small. The downstream output Bragg reflector with length $l_{1D} =$ 20 cm had a 1D corrugation with a period of 0.2 cm and a depth of 0.07 cm and formed the feedback loop via coupling of two counterpropagating partial waves of TEM types in the operating frequency band.

After passing the interaction space, the REBs propagated together with the generated rf pulses to the graphite collector. Separation of electrons and high-power rf radiation were implemented directly at the collector surface. The surface was inclined at the angle of 45° to the magnetic field lines, and as a result, the rf pulse was reflected by an angle of 90° while the REBs were dumped by the collector [Fig. 1(a)]. Finally, the rf pulse was emitted from each channel separately through Teflon output vacuum windows.

For theoretical analysis of the FEM described above, we assume that the magnetically guided beam move along the z axis near the symmetry plane with the longitudinal velocity $v_{||} = \beta_{||} c$ and oscillate in the planar wiggler of the period d_w with the bounce frequency $\Omega_b = h_w v_{||}$, $h_w = 2\pi/d_w$. The radiation field can be presented as a sum of the four quasioptical beams (1), and the electron beams interact with the forward wave C_z^+ under the wiggler resonance (synchronism) condition $\omega - h v_{||} = \Omega_b$. As opposed to previous works [4,10–12], the theoretical model developed in this Letter allows the description of the formation of a self-consistent structure of the rf field over all space coordinates (x, y, and z). Based on the concept of surface magnetic currents [14,15], the process of partial wave scattering inside the 2D Bragg structure and amplification of the synchronous wave by the beam can be described as

$$i\frac{\partial^2 C_z^+}{\partial Y^2}+\frac{\partial C_z^+}{\partial Z}+\frac{\partial C_z^+}{\partial \tau}=i\alpha_{2D}(C_x^+ + C_x^-)\times[\delta(Y)+\delta(Y-L_y)]+\rho(X;Y)J,$$

$$i\frac{\partial^2 C_z^-}{\partial Y^2}-\frac{\partial C_z^-}{\partial Z}+\frac{\partial C_z^-}{\partial \tau}=i\alpha_{2D}(C_x^+ + C_x^-)\times[\delta(Y)+\delta(Y-L_y)],$$

$$i\frac{\partial^2 C_x^\pm}{\partial Y^2}\pm\frac{\partial C_x^\pm}{\partial X}+\frac{\partial C_x^\pm}{\partial \tau}=i\alpha_{2D}(C_z^+ + C_z^-)\times[\delta(Y)+\delta(Y-L_y)], \quad (4)$$

where $\delta(Y)$ is the delta function, $\rho(X;Y)$ defines the transverse distribution of the beam electron particle density, and $\alpha_{2D}=a_{2D}h/8G$ is the wave-coupling coefficient of the 2D Bragg structure [4]. The rf current $J(X,Y,Z,\tau)=(1/\pi)\int_0^{2\pi}e^{-i\theta}d\theta_0$ can be found from the averaged equations of electron motion derived for the electron phase $\theta=\bar{\omega}t-hz-h_w z$ with respect to the synchronous partial wave C_z^+

$$\left(\frac{\partial}{\partial Z}+\beta_{\|}^{-1}\frac{\partial}{\partial \tau}\right)^2\theta=\mathrm{Re}[C_z^+ e^{i\theta}]. \quad (5)$$

A conventional downstream 1D Bragg structure [Fig. 1(a)] having a single-periodical corrugation $a=a_{1D}\cos h_{1D}z$ ($h_{1D}=2\pi/d_{1D}$, d_{1D}, and $2a_{1D}$ are the corrugation period and depth, correspondingly) under the Bragg resonance condition

$$2h\approx h_{1D} \quad (6)$$

provides mutual scattering of the two counterpropagating partial waves $C_z^\pm$, which can be described by the equations

$$i\frac{\partial^2 C_z^+}{\partial Y^2}+\frac{\partial C_z^+}{\partial Z}+\frac{\partial C_z^+}{\partial \tau}=i\alpha_{1D}C_z^-[\delta(Y)+\delta(Y-L_y)]+\rho(X;Y)J,$$

$$i\frac{\partial^2 C_z^-}{\partial Y^2}-\frac{\partial C_z^-}{\partial Z}+\frac{\partial C_z^-}{\partial \tau}=i\alpha_{1D}C_z^+[\delta(Y)+\delta(Y-L_y)], \quad (7)$$

where $\alpha_{1D}=a_{1D}h/2G$ is the wave-coupling coefficient of the 1D structure [7]. Amplification of the synchronous wave in the regular section of the resonator is also described by Eqs. (5) and (7) when $\alpha_{1D}=0$, since wave coupling here is absent. In Eqs. (4), (5), and (7), we used the following dimensionless variables and parameters: $\tau=G\bar{\omega}t$, $Z=G\bar{\omega}z/c$, $X=G\bar{\omega}x/c$, $Y=\sqrt{2G\bar{\omega}}y/c$, and $C_{x,z}^\pm=C_{x,z}^\pm e\mathrm{K}\mu/\gamma mc\bar{\omega}G^2$, where γ is the relativistic Lorentz factor, $\mathrm{K}=2\alpha_w g/(1-g^2)$ is the electron-wave-coupling parameter, $\mu=\gamma^{-2}+2\alpha_w^2(1+3g^2)/(1-g^2)^3$ is the inertial bunching parameter [7], $\alpha_w=eH_w/2h_w\gamma mc^2$, $G=[eI_0\lambda^2\alpha_w^2\mu g^2/2\pi\gamma mc^3 a_0(1-g^2)]^{1/3}$ is the gain parameter, I_0 is the linear beam current density, $g=\omega_H/\Omega_b$, ω_H is the electron cyclotron frequency, and $\bar{\omega}=h_{2D}c$ is the Bragg frequency used as the carrier frequency. Simultaneous fulfillment of conditions (3) and (6) takes place when $d_{2D}\approx 2d_{1D}$.

Simulations were performed assuming that external energy fluxes are absent, the partial wave amplitudes are 0 at the corresponding boundaries, and these waves are not reflected from the edges of the different waveguide sections. At the entrance of the interaction space, we considered the REBs as monoenergy and nonmodulated (see Refs. [3,4]).

The results of simulations of the oscillation buildup for a microwave system geometry and electron beam parameters very close to the experimental conditions described above are shown in Fig. 2. These simulations demonstrate the establishment of the steady-state single-frequency operation regime [Fig. 2(a)]. The rf field distribution over the y coordinate corresponds to the excitation of the designed TEM mode. The simulations also prove that the upstream 2D Bragg structure provides synchronization of radiation from various parts of each oversized sheet REB as well as for the two parallel beams. Thus, application of the 2D Bragg structure allowed perfect phase correlation over the transverse x coordinate for the output radiation front associated with the partial wave C_z^+ to be achieved [see Fig. 2(b)]. It is also important to emphasize that this wave in the steady-state generation regime has practically uniform

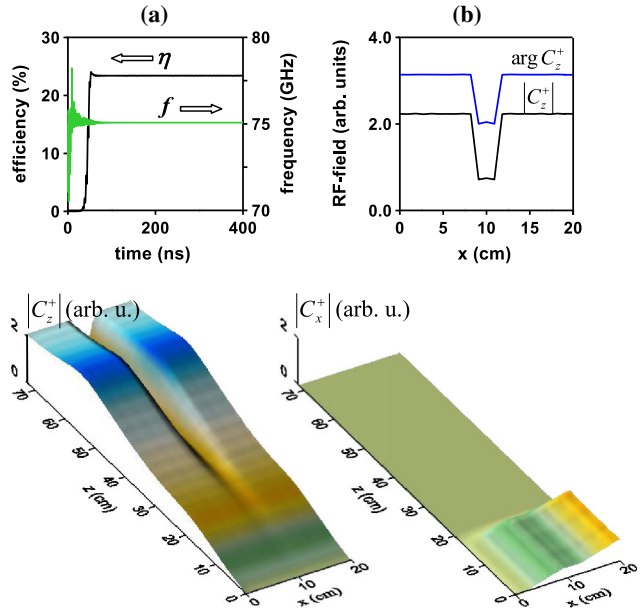

FIG. 2. Simulation of oscillation buildup in the two-beam planar FEM. (a) Establishment of steady-state oscillations under the optimal parameters: time dependence of the FEM efficiency $\eta(t)$ and oscillation frequency $f(t)$. (b) Transverse distribution of the amplitude $|C_z^+(x)|$ and phase $\arg C_z^+(x)$ of the forward resonant wave at the output of the interaction space. Spatial structures of the partial waves (c) $|C_z^+(x,z)|$ and (d) $|C_x^+(x,z)|$ (wave of synchronization) in the stationary regime.

field distribution over the transverse coordinate x in the regions of beam propagation [see Fig. 2(c)], which ensures the same conditions for energy extraction from all the beam electrons and rather high electron efficiency. It should be noted, however, that some change (jitter) of electron energy, which occurred during an individual beam pulse and/or from pulse to pulse, can result in a stepwise variation of the radiation frequency when resonator modes with different numbers of the field variation over the longitudinal z coordinate can be excited in different pulses.

In the initial series of the experiments described in Ref. [12], the two planar channels driven by the parallel-sheet REBs were entirely separated along all the interaction space by a baffle and thus operated practically independently. In this Letter, we describe experiments when the baffle was removed inside of the 2D Bragg structure in the upstream reflector. Under these conditions, both channels are strongly coupled via the transverse energy fluxes arising in this structure. As a result, complete synchronization of radiation from these two channels takes place.

In the experiments, the rf generation was shifted by ~0.5 μs from the beginning of beam injection [Fig. 3(a)] and started when the beam current exceeds the level of ~0.5 kA, which is in good agreement with the self-excitation threshold found in the time-domain analysis given above. Maximum radiation power was observed at the wiggler field of 0.12–0.14 T and the axial magnetic field of about 1.2 T. Stable narrow-band rf generation at a frequency close to the frequency of one of the longitudinal eigenmodes of the hybrid Bragg resonator was obtained simultaneously in both channels under the optimal value of the experiment parameters [see Fig. 3(b)]. Measurements showed that in most of the pulses, the eigenmode at the frequency of 74.96 GHz was excited [Fig. 3(b)]. The width of the radiation spectrum is about 20 MHz and close to the theoretical limit for the radiation pulse duration that was about 100 ns in the current series of the experiments. The microwave power of about 30–50 MW was measured by using a calorimeter and calibrated hot-carrier detectors. The angular distribution of the output radiation was analyzed by registering the illumination of a neon bulb panel positioned at various distances from the FEM output windows. The resulting directional diagram indicates the high content of the fundamental TEM mode in the output radiation.

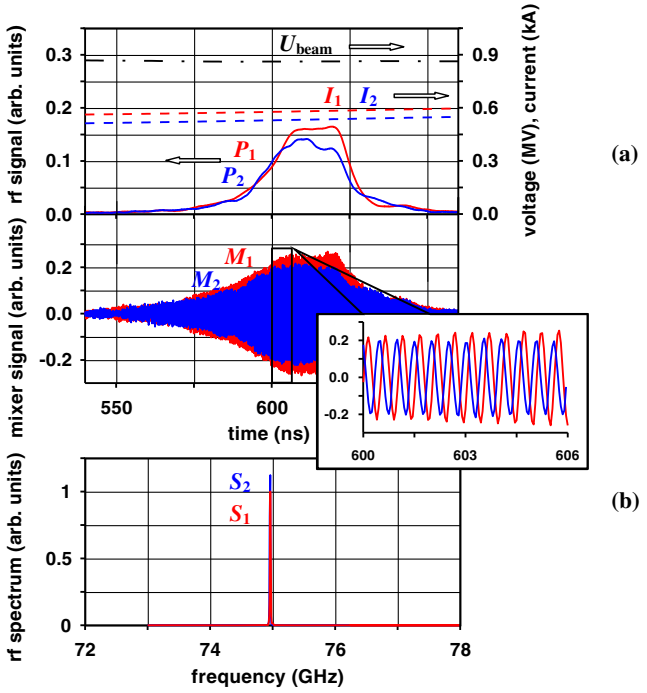

FIG. 3. Results of experimental studies on the planar two-beam 75 GHz FEM. Typical oscilloscope traces of (a) accelerating voltage U_{beam} and currents of the electron beams $I_{1,2}$ during the microwave pulses, with signals from rf power detectors $P_{1,2}$ (top) and heterodyne mixers $M_{1,2}$ (bottom). (b) Corresponding frequency spectra of the rf pulses $S_{1,2}$ (signals from channel 1 are shown by red and from channel 2 by blue, correspondingly). In the zoomed-in inset of Fig. 3(a), the synchronized signals from the heterodyne mixers are shown in a large time scale.

To analyze the limitation of the radiation pulse duration, we controlled the time behavior of the plasma inside the FEM channels. The light emission from the plasmas was registered by fiber-optical guides and photomultiplier tubes. The measurements indicated that the density of the plasma arising in the interaction region during the microwave pulse is close to the limit at which its influence on the rf waves of the resonator is substantial.

Coherent wave generation in the two channels in a typical shot is illustrated by Fig. 3(a). From the time dependence of the heterodyne signals, one can see the establishment of the oscillation regime that is characterized by narrow-band generation at the single frequency [Fig. 3(b)] with stable correlation of the radiation phases in both channels [see the zoomed-in inset in Fig. 3(a)]. Thus, the phase synchronization of radiation generated by the two parallel-sheet beams has been experimentally demonstrated. It should be noted that the output rf power from each channel measured in these experiments was at the same level as in the previous experiments with separated channels [12].

We should note that in the final stage of the previous experiments described in Ref. [12], the separating baffle was removed from the collector side of the interaction space, which results in the weak diffraction coupling between the two channels. In this case, different oscillating regimes were observed. In a large number of pulses, the frequencies of generation in the steady-state regime in both channels were different. Nevertheless, in some shots, during the time when the pulses in both channels were overlapped, the phase correlation between the rf signals was observed. However, those synchronization regimes were sporadic and unstable, and they changed with even small variations of the beam parameters.

In summary, implementation of 2D distributed feedback allowed the synchronization of stable narrow-band

oscillation regimes in two coupled FEMs driven by two parallel relativistic electron beams with 75 GHz output power of 30–50 MW in each channel. The noise level in the experimentally recorded radiation spectrum was less than 25 dB [see Fig. 3(b)]. We would like to emphasize that at the present stage, we realized powerful FEMs with microwave systems having an entire cross section of 45×2.5 wavelengths. The oversize factor of such systems is comparable with the cavities of modern megawatt-power gyrotrons [16–19]. The theoretical analysis demonstrates that this novel feedback mechanism possesses significant potential for further increase of the transverse size of the interaction space to achieve ultra-high-power coherent wave generation from spatially extended active media, including multibeam schemes. Note also that two-beam systems provide many opportunities for further developments. For example, if the radiation frequency in the two channels would be a little different, it would be possible to arrange space scanning of the output radiation pattern direction similar to that described in Ref. [20]. We also plan to use the second channel for observation of stimulated backscattering of radiation from the first channel to produce terahertz waves [21].

This work is supported partially by RSCF Project No. 14-12-00610 for development of frequency selecting diagnostics and the RFBR under Grants No. 16-08-00811 and No. 16-02-00890 for theoretical studies and design of the experimental facility. The reconstruction of the ELMI device for two channel experiments was done under financial support by the State through Project No. RFMEFI61914X0003.

[1] A. V. Arzhannikov, V. S. Nikolaev, S. L. Sinitsky, A. V. Smirnov, M. V. Yushkov, and R. P. Zotkin, J. Appl. Phys. **72**, 1657 (1992).
[2] A. V. Arzhannikov, V. T. Astrelin, A. V. Burdakov, I. A. Ivanov, V. S. Koidan, K. I. Mekler, V. V. Postupaev, A. F. Rovenskikh, S. V. Polosatkin, and S. L. Sinitskii, JETP Lett. **77**, 358 (2003).
[3] N. S. Ginzburg, N. Yu. Peskov, and A. S. Sergeev, Opt. Commun. **96**, 254 (1993).
[4] N. S. Ginzburg, N. Y. Peskov, A. S. Sergeev, A. D. R. Phelps, I. V. Konoplev, G. R. M. Robb, A. W. Cross, A. V. Arzhannikov, and S. L. Sinitsky, Phys. Rev. E **60**, 935 (1999).
[5] A. Yariv, *Quantum Electronics* (Wiley, New York, 1975).
[6] H. Kogelnik and C. V. Shank, J. Appl. Phys. **43**, 2327 (1972).
[7] V. Bratman, G. Denisov, N. Ginzburg, and M. Petelin, IEEE J. Quantum Electron. **19**, 282 (1983).
[8] N. S. Ginzburg, V. R. Baryshev, A. S. Sergeev, and A. M. Malkin, Phys. Rev. A **91**, 053806 (2015).
[9] I. V. Konoplev, P. McGrane, W. He, A. W. Cross, A. D. R. Phelps, C. G. Whyte, K. Ronald, and C. W. Robertson, Phys. Rev. Lett. **96**, 035002 (2006).
[10] I. V. Konoplev *et al.*, Phys. Rev. E **76**, 056406 (2007).
[11] A. V. Arzhannikov *et al.*, JETP Lett. **87**, 618 (2008).
[12] A. V. Arzhannikov, N. S. Ginzburg, V. Yu. Zaslavsky, P. V. Kalinin, N. Yu. Peskov, A. S. Sergeev, S. L. Sinitsky, V. D. Stepanov, and M. Thumm, Tech. Phys. Lett. **39**, 801 (2013).
[13] N. S. Ginzburg, N. Yu. Peskov, A. S. Sergeev, A. V. Arzhannikov, and S. L. Sinitsky, Nucl. Instrum. Methods Phys. Res., Sect. A **475**, 173 (2001).
[14] B. Z. Katsenelenbaum *et al.*, *Theory of Nonuniform Waveguides: The Cross-Section Method*, IEEE Electromagnetic Waves Series Vol. 44 (IET, London, 1998).
[15] N. F. Kovalev, I. M. Orlova, and M. I. Petelin, Radiophys. Quantum Electron. **11**, 449 (1968).
[16] A. G. Litvak, G. G. Denisov, V. E. Myasnikov, E. M. Tai, E. A. Azizov, and V. I. Ilin, J. Infrared Millimeter Terahertz Waves **32**, 337 (2011).
[17] K. Sakamoto, A. Kasugai, K. Kajiwara, K. Takahashi, Y. Oda, K. Hayashi, and N. Kobayashi, Nucl. Fusion **49**, 095019 (2009).
[18] J. F. Tooker, P. Huynh, K. Felch, M. Blank, P. Borchardt, and S. Cauffman, Fusion Eng. Des. **88**, 521 (2013).
[19] A. Schlaich, G. Gantenbein, S. Illy, J. Jelonnek, and M. Thumm, IEEE Trans. Electron Devices **62**, 3049 (2015).
[20] K. A. Sharypov *et al.*, Appl. Phys. Lett. **103**, 134103 (2013).
[21] A. V. Arzhannikov, N. S. Ginzburg, G. G. Denisov, P. V. Kalinin, N. Yu. Peskov, A. S. Sergeev, and S. L. Sinitskii, Tech. Phys. Lett. **40**, 730 (2014).